Article

Simulation of Underwater Explosions Initiated by High-Pressure Gas Bubbles of Various Initial Shapes: Supplements

Le Cao [1,*], Wenli Fei [1], Holger Grosshans [2] and Nianwen Cao [1]

[1] Key Laboratory for Aerosol-Cloud-Precipitation of China Meteorological Administration, Nanjing University of Information Science and Technology, Nanjing 210044, China; wenli.fei@nuist.edu.cn (W.F.); nwcao@nuist.edu.cn (N.C.)

[2] Institute of Mechanics, Materials and Civil Engineering, Université catholique de Louvain, Louvain-la-Neuve 1348, Belgium; holger.grosshans@uclouvain.be

* Correspondence: le.cao@nuist.edu.cn; Tel.: +86-025-5869-9771.

1. Validation Simulations

Scenario 1:

A 1-D simulation of the interaction between a gas shock and a gas-water interface was taken from [1] to validate the model. The configuration of the simulation scenario is shown in Fig. S1. The non-dimensional length of the computational domain is 1.0. The left side of the computational domain is filled with gas, while the water medium stays on the right side. When $t = 0.0$, the gas-water interface and the shock are initially located at $x = 0.5$.

The initial values of the fluid properties are listed in Tab. S1, in which the pressure ratio of gas and water is assumed as 1000:1. For a detailed description of this simulation scenario, please refer to [1].

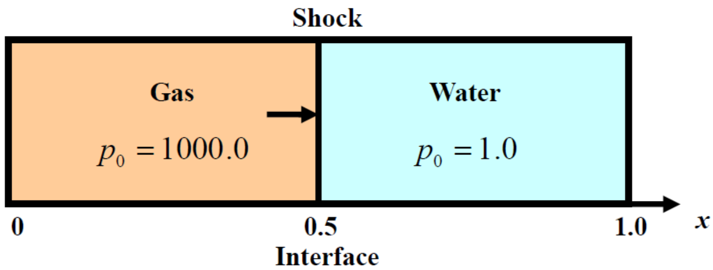

Figure S1. The initial setup of the 1-D simulation of the gas shock impacting on the gas-water interface, taken after [1].

Table S1. The initial values of fluid properties of the 1-D numerical test.

	Pressure	Velocity	Density
Gas (pre-shock)	1.0	0.0	1.0×10^{-3}
Gas (post-shock)	1000.0	911.9	5.97×10^{-3}
Water	1.0	0.0	1.0

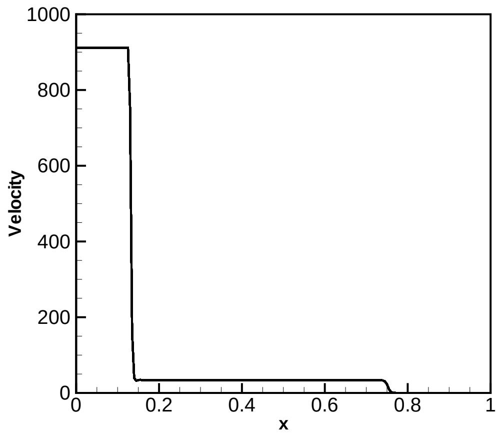

(**a**) Velocity

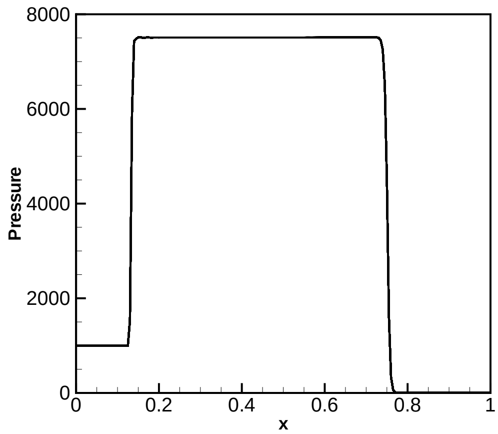

(**b**) Pressure

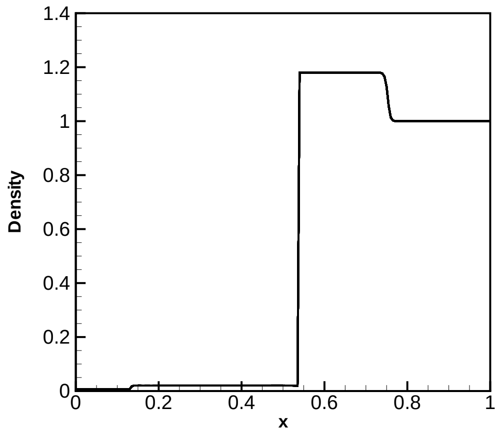

(**c**) Density

Figure S2. The distribution of velocity, pressure and density along x direction after 350 time steps of computations by using the present 3-D model.

Figure S2 shows the computational results obtained at the 350$^{\text{th}}$ time step by using the present 3-D model, which can be compared with the earlier 1-D model results [1]. It was found that after the impinging of the gas shock on the gas-water interface, the refraction of shock occurs, leading to a transmitted shock in the water as well as a reflected shock in the gas. In Figs. S2(a) and (b), it was seen that at this time point, the reflected shock wave on the gas side has moved to the location $x = 0.12$, and the transmitted underwater shock is located at $x = 0.76$. Figure S2(b) also shows that due to the shock refraction at the interface, both of the pressure of the gas and the water have increased significantly, reaching a value of 7508, which is about 7.5 times of the incident shock pressure. Moreover, due to the compression of the transmitted shock wave, the density of the aqueous medium also increases

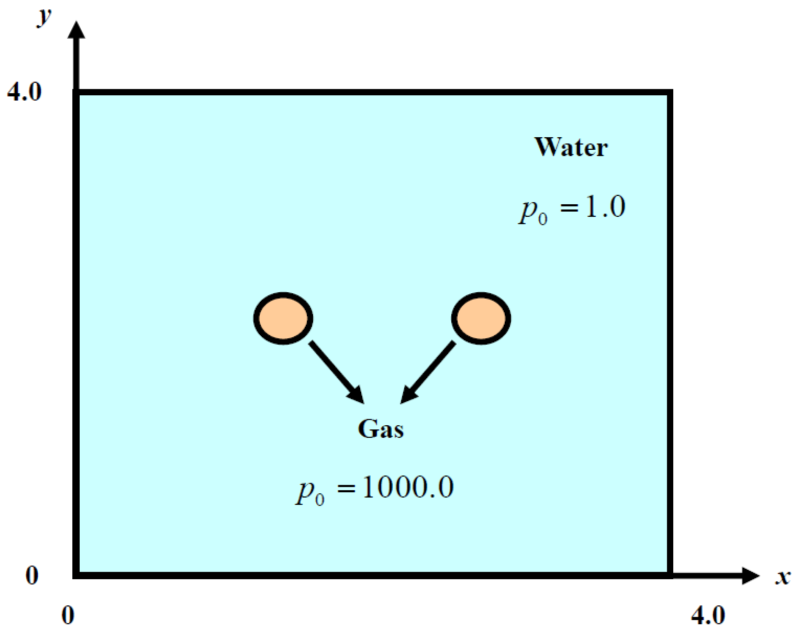

Figure S3. The initial configuration of the 2-D double underwater explosion simulation, taken after [2].

Table S2. The initial conditions of the 2-D validation simulation.

	Pressure	Horizontal Velocity (u)	Vertical Velocity (v)	Density
Gas	1000.0	0.0	0.0	1000.0
Water	1.0	0.0	0.0	1000.0

to approximately 1.2 times of the original value (see Fig. S2c). The simulated results are in good agreement with the theoretical calculation and the previous model results obtained by Liu *et al.* [1] using the modified ghost fluid method (MGFM) combined with the level set method, with a deviation of only 0.2%. Thus, the reliability of the present model in capturing the gas shock impacting with the gas-water interface is verified.

Scenario 2:

A two-dimensional simulation of a double underwater explosion initiated by two spherical high-pressure gas bubbles was also performed to verify the correctness of the present 3-D model. The configuration of the simulation scenario is displayed in Fig. S3. The non-dimensional size of the computational domain is $[0.0, 4.0] \times [0.0, 4.0]$, and the number of grid nodes is 201×201. Two highly-pressurized bubbles with a radius of 0.3 are submerged in a water environment, and the centers of these two bubbles are located in the positions of (1.4, 2.0) and (2.6, 2.0).

The initial values of the parameters for gas and water are listed in Tab. S2, in which the pressure ratio of gas and water is 1000:1. Besides, the high-pressure gas bubbles and the water medium are assumed initially quiescent. A detailed description of this simulation scenario is provided in [2].

The evolutions of the pressure field at different time points are shown in Figs. S4(a) - (c), which can be compared with the earlier model results obtained by Wang *et al.* [2] using real ghost fluid method (RGFM) and the construction of artificial velocity field. It is seen that due to the initial high-pressure gas inside the bubbles, two outward compressive shock waves are formed and transmitted radially in the water (see Fig. S4a). Later, the intersection of these two outward shocks occurs (see Fig. S4b). As a result, the shocks are reflected, traveling towards the bubbles. Then the reflected shocks collide with the expanding bubbles (see Fig. S4c), leading to the transmission of a compressive shock wave inside the bubbles. In contrast to that, rarefaction waves are formed on the water side (see Fig. S4c), causing a pressure drop in the regions near the gas bubbles. The wave types captured in our 3-D simulations as well as the locations of the wave fronts are in good consistence with the earlier model results obtained in [2], which again proves the correctness of the model used in the present study.

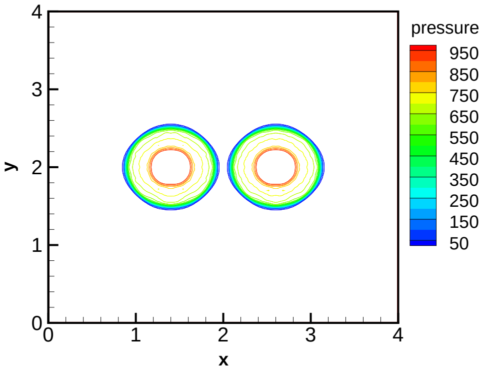

(**a**) $t = 3.7 \times 10^{-2}$

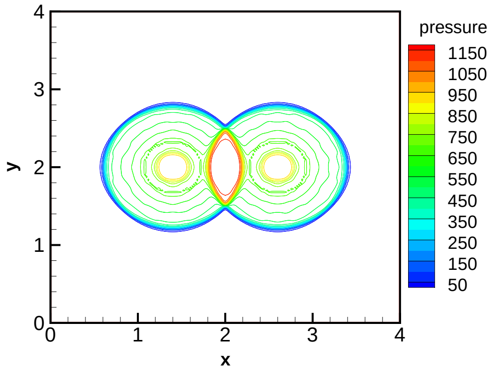

(**b**) $t = 9.2 \times 10^{-2}$

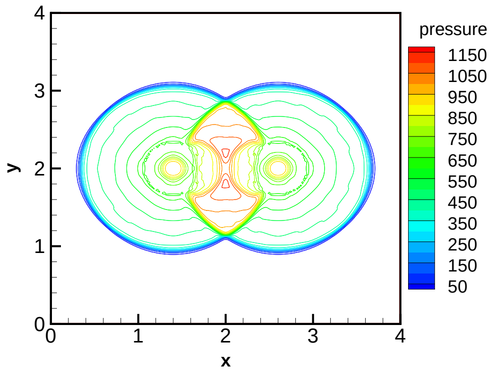

(**c**) $t = 1.5 \times 10^{-1}$

Figure S4. The evolutions of the pressure field of the 2-D validation case at different time points by using the 3-D model.

2. Comparison with a Finer Mesh Size Simulation

In this section, we show the results of the bullet-like shaped bubble simulation (Scenario 4) with the mesh size of $61 \times 61 \times 61$ and $81 \times 81 \times 81$ at the same time (see Figs. S5 and S6).

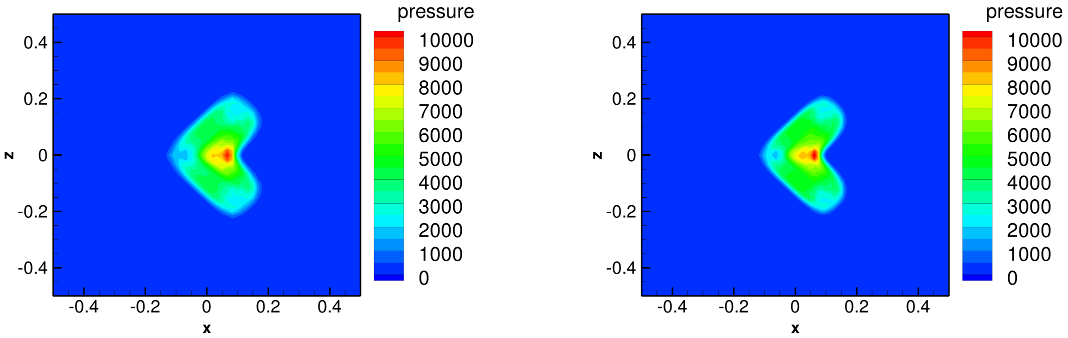

(**a**) $t = 0.006$

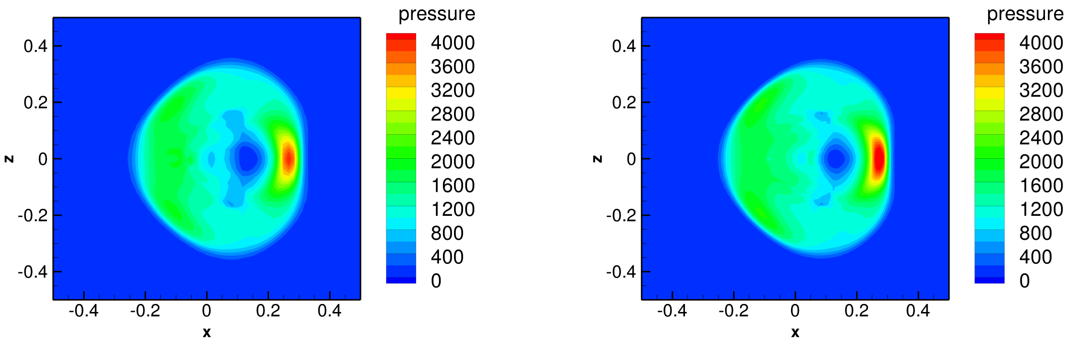

(**b**) $t = 0.03$

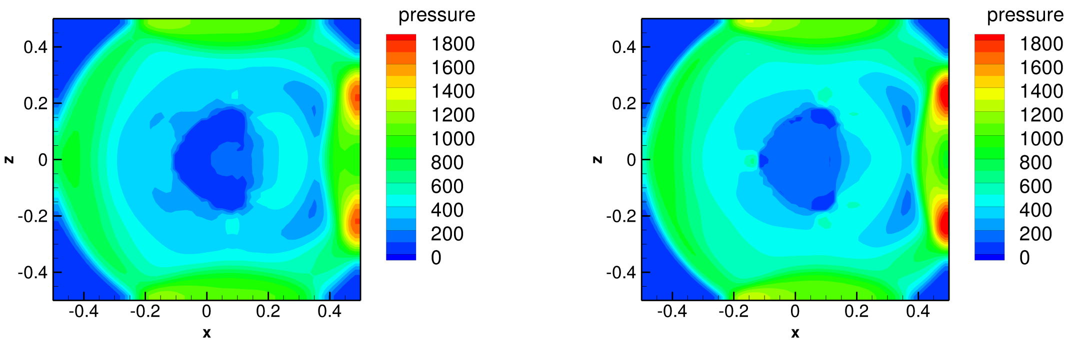

(**c**) $t = 0.08$

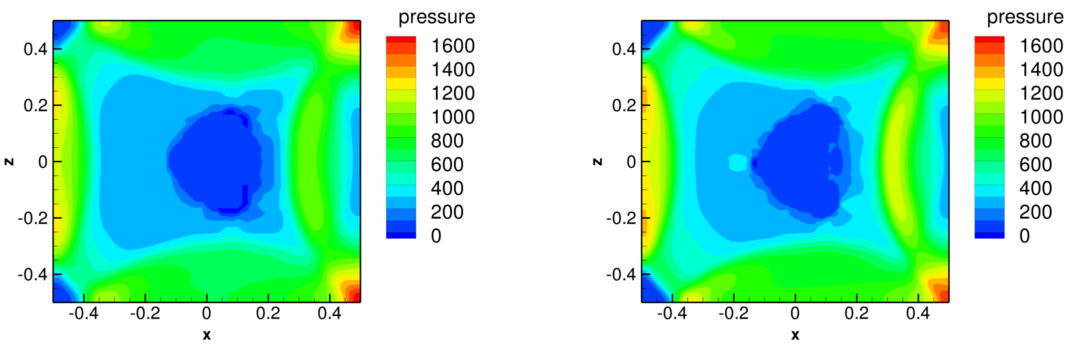

(**d**) $t = 0.10$

Figure S5. The temporal evolution of the pressure field for an initially bullet-like bubble in slice plots ($y = 0$) (Scenario 4); mesh size: (left) $61 \times 61 \times 61$; (right) $81 \times 81 \times 81$.

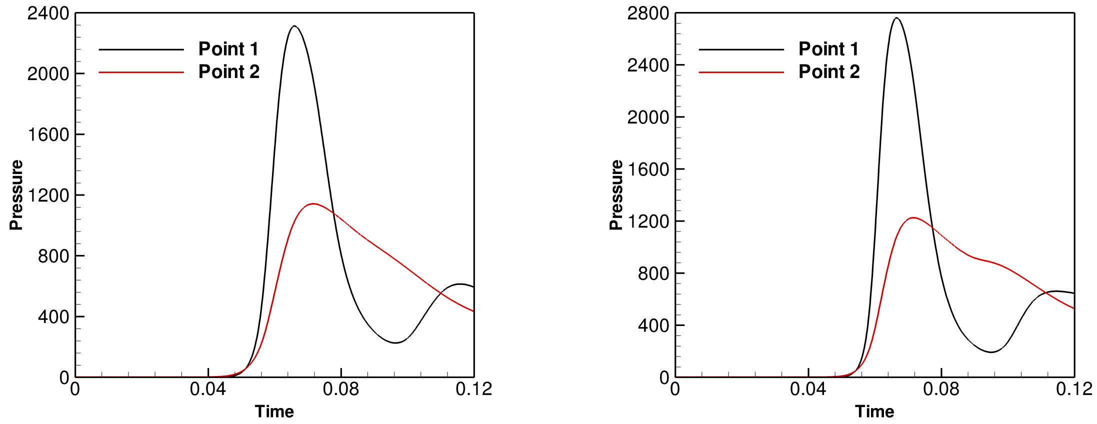

Figure S6. The pressure history recorded at the boundaries of the computational domain for an initially bullet-like bubble (Scenario 4); mesh size: (left) $61 \times 61 \times 61$; (right) $81 \times 81 \times 81$.

It is not surprising to find that the finer-mesh simulation captures more details of the flow field (see Fig. S5). Besides, it is also found in Fig. S6 that in the $81 \times 81 \times 81$ computation, a higher peak value of pressure is recorded at the lateral boundary. It is because that in the finer-mesh computation, the numerical diffusion is weaker due to the smaller grid space than that in the coarse-mesh simulation. As a result, the sudden jump of the pressure can be kept, while this sharp increase of pressure is smoothed out by the relatively larger numerical diffusion in the coarser-mesh computation. However, it can be also seen from Figs. S5 and S6 that the results of these two simulations such as the location of the shocks and the time-dependent pressure curves are quite similar. Moreover, the $81 \times 81 \times 81$ simulation costs more than 8 days while the $61 \times 61 \times 61$ case lasts only three days to finish. Thus, the choice of the mesh size ($61 \times 61 \times 61$) adopted in the present study is a result from the balance between the computational resources and the numerical accuracy.

3. Asymmetry of the Computational Results

We show the pressure distribution along the x direction (when $y = 0$ and $z = 0$) at different time (Fig. S7) as well as the time-dependent curves at the left and right boundaries (Fig. S8), to see the difference of pressure in opposite directions. We take the spherical bubble case for example.

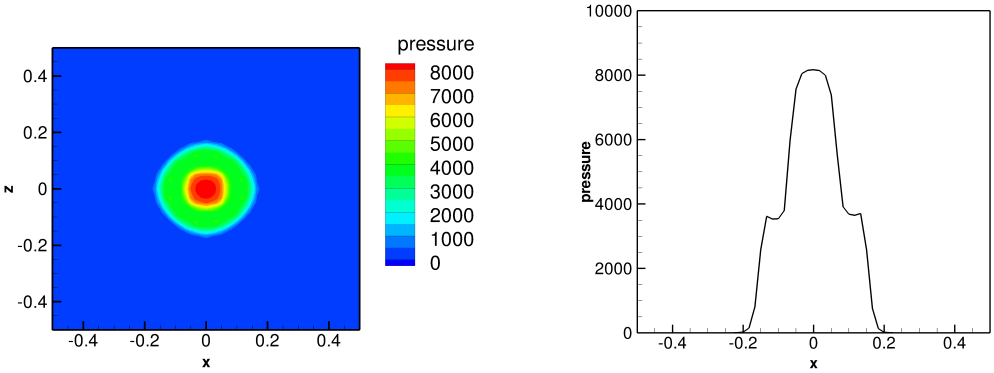

(**a**) $t = 0.006$

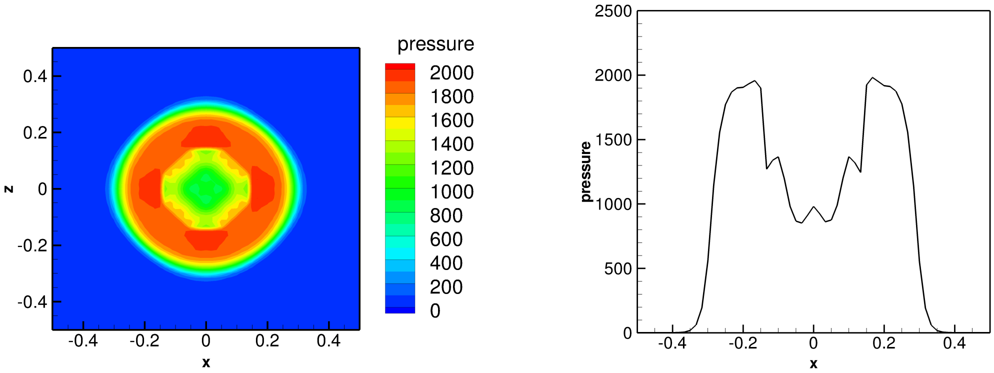

(**b**) $t = 0.03$

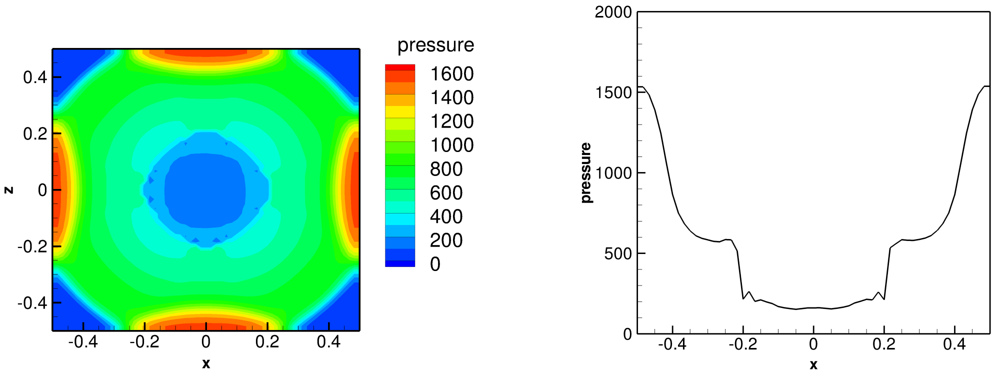

(**c**) $t = 0.08$

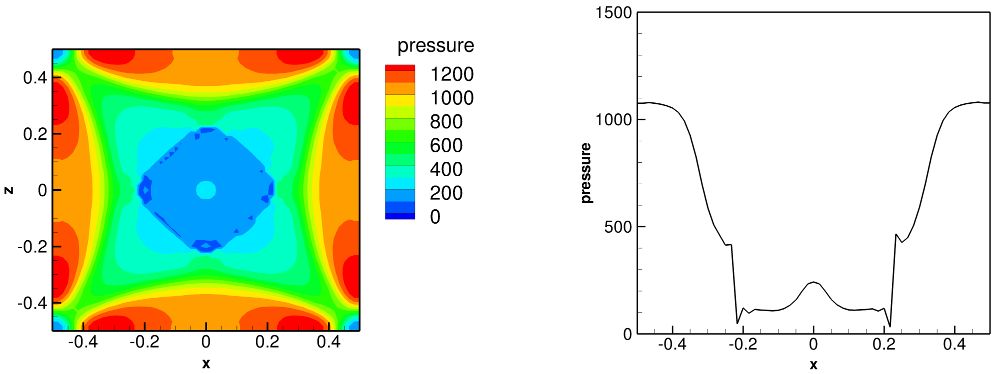

(**d**) $t = 0.10$

Figure S7. The distribution of pressure along the x direction ($y = 0$ and $z = 0$) (Scenario 1).

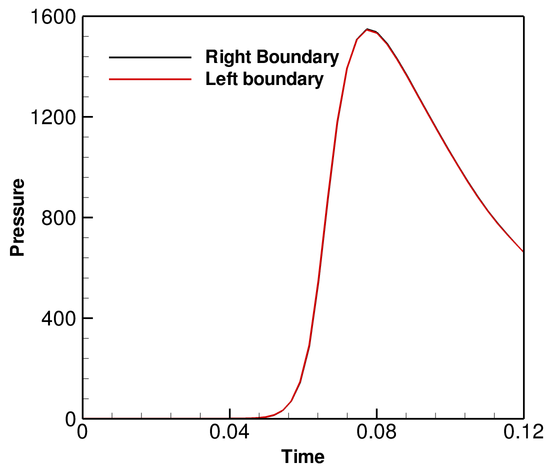

Figure S8. The time-dependent curves of pressure recorded at the left and right boundaries of the computational domain (Scenario 1).

From the comparisons shown above, we can see that this asymmetry affects mostly the low-pressure regions of the computational domain (see Fig. S7). In contrast to that, the propagating high-pressure shock is slightly influenced. It is also seen from Fig. S8 that the influence of this asymmetry on the pressure felt by the lateral domain boundaries in opposite directions is small, with a deviation less than 1%.

References

1. Liu, T.; Khoo, B.; Yeo, K. Ghost fluid method for strong shock impacting on material interface. *J. Comput. Phys.* **2003**, *190*, 651 – 681.
2. Wang, C.W.; Liu, T.G.; Khoo, B.C. A real ghost fluid method for the simulation of multimedium compressible flow. *SIAM J. Sci. Comput.* **2006**, *28*, 278–302.